

Hydrothermal synthesis of 11 Å tobermorite from chicken eggshells, rice husks, and soda-lime-silica glasses for wastewater treatment application

V. LORYUENYONG^{a,b,*}, T. NGOYJANSRI^a, P. YANTREESINGHA^a, S. LEELAWANNAKHET^a, A. BUASRI^{a,b}

^aDepartment of Materials Science and Engineering, Faculty of Engineering and Industrial Technology, Silpakorn University, Nakhon Pathom 73000, Thailand

^bNational Center of Excellence for Petroleum, Petrochemicals and Advanced Materials, Chulalongkorn University, Bangkok 10330, Thailand

The objective of this research is to transform discarded or biomass waste materials into a resource for environmental cleanliness purposes. Al-substituted tobermorite was synthesized from inexpensive waste materials such as eggshells, rice husks and glass cullets. The synthesis was conducted using alkaline hydrothermal method and the following optimal condition: 150°C for 48 hours and the molar ratio of $\text{CaO}/(\text{SiO}_2 + \text{Al}_2\text{O}_3) = 0.83$ and $\text{Al}_2\text{O}_3/(\text{Al}_2\text{O}_3 + \text{SiO}_2) = 0$. Based on FTIR, Raman spectroscopy, XRD, SEM and DSC analysis, high-crystalline 11 Å tobermorite with large specific surface area was obtained from eggshells and rice husks as CaO and SiO₂ powder reagents, respectively. The Pb²⁺ and Cd²⁺-uptake capacities were influenced by the amount of tobermorite, the specific surface area, as well as the tobermorite crystallinity.

(Received September 11, 2013; accepted May 15, 2014)

Keywords: Tobermorite, Al substitution, Hydrothermal synthesis, Wastes, Ion exchange

1. Introduction

Water pollution is one of the crucial and ongoing problems worldwide. One of the ways to reduce the impact of such pollution is to efficiently treat the wastewater. As a result, many treatment methods, such as ion exchange and adsorption, have been developed for the separation of polluting species. Porous inorganic solids, i.e., activated carbon, have found great utility in various adsorption and catalytic applications because of their large specific surface area. Nevertheless, ion-exchanging materials have also been known as a good alternative to significantly reduce toxic heavy metals from contaminated water. Examples include zeolite and calcium silicate hydrate (C-S-H) materials.

The C-S-H compounds of tobermorite group are well known in cement industry [1, 2]. They form when cement reacts with water and play an important role in the binding process as well as an increase in mechanical strength. Several tobermorite compounds such as Al-substituted 11 Å tobermorite exhibit cation exchange behavior as well as selective cation adsorption properties. Subsequently, these materials have been receiving attentions as a cation exchanger in hazardous waste disposal. Previous researches have reported that Al-substituted 11 Å tobermorite, whose ideal composition is $\text{Ca}_5\text{Si}_6\text{O}_{18}\text{H}_2 \cdot 4\text{H}_2\text{O}$, can be synthesized under alkaline hydrothermal conditions at temperatures

between 80 and 200°C and with the molar ratio of the oxide raw materials as following: $0.8 < \text{CaO}/(\text{SiO}_2 + \text{Al}_2\text{O}_3) < 0.85$ and $0 < \text{Al}_2\text{O}_3/(\text{SiO}_2 + \text{Al}_2\text{O}_3) < 0.17$ [3-6].

Tobermorite is a naturally occurring layered C-S-H mineral. To facilitate the description of the silicate structure of 11 Å tobermorite, Qⁿ notation will be used, in which the symbol Q represents one SiO₄⁴⁻ tetrahedron and the superscript n denotes the number of other Q units to which it is bonded. As a result, Q⁰ refers to isolated SiO₄⁴⁻ group, Q¹ to end group in silicate chain, Q² to middle group in chain and Q³ to SiO₄⁴⁻ group linking between two silicate chains [7-10].

The synthesis of tobermorite materials is typically based on the use of analytical grade reagents. Recent efforts have been made to replace reagent- or laboratory-grade feedstock constituents with municipal solid wastes. Coleman [7, 8], for example, has transformed recycled glasses and newsprint recycling residue into tobermorite by heating in a sealed stainless steel container. This tobermorite can effectively remove heavy metals from ground- or wastewater streams.

In this paper, the authors, therefore, explored the feasibility of using various waste materials such as eggshells, rice husks, and discarded soda-lime-silica glass containers for the one-step hydrothermal synthesis of 11 Å Al-substituted tobermorite. The obtained products were compared with those synthesized from reagent-grade oxide powders.

2. Experimental details

2.1 The preparation of raw materials

The locally-supplied waste raw materials, such as chicken eggshells, rice husks, and glass cullets from discarded soda-lime-silica glass containers, were used as a source of CaO, SiO₂, and SiO₂, respectively. All of the raw materials were crushed and washed prior to use. SiO₂ powders (~98%) could be extracted from rice husks by refluxing with 3M HCl aqueous solution (100g:500ml) at 60°C for 3 hrs, washed repeatedly using

deionized water, and finally calcined at 800°C for 6 hrs. CaO powders (~98%) from chicken eggshells were obtained via direct calcination at 1000°C for 3 hrs. Glass cullets (~64% SiO₂ and ~14% CaO), on the other hand, were ball milled and used as received. All of the obtained oxide materials were then ground using porcelain mortar with a pestle and sieved before used as starting materials. Oxide analyses and particle size analyses of starting materials were performed, using X-ray fluorescence spectroscopy (XRF, Philips PW2400) and Master Sizer Particle Size Analysis (Coulter LS100), respectively. The results are illustrated in Table 1 and Fig. 1.

Table 1. Composition of starting raw materials.

Oxide	Mass (%)		
	CaO from eggshells	SiO ₂ from rice husks	Glass cullets
Na ₂ O	-	0.086	15.451
MgO	1.221	0.224	2.986
Al ₂ O ₃	0.025	0.062	1.394
SiO ₂	0.08	98.238	64.157
P ₂ O ₅	0.603	0.07	0.029
SO ₃	0.409	0.28	0.069
Cl	-	-	0.049
K ₂ O	0.022	0.1	0.216
CaO	97.628	0.888	14.077
TiO ₂	-	0.031	0.098
Fe ₂ O ₃	-	0.02	0.434
SrO	0.012	-	0.009
ZnO ₂	-	-	0.017

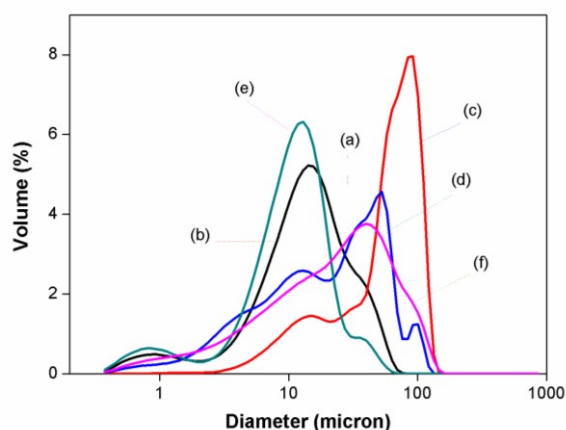


Fig. 1. Particle size distribution of starting raw materials: (a) Al₂O₃, (b) CaO, (c) SiO₂, (d) SiO₂ from rice husk, (e) CaO from egg shells and (f) glass cullets. The average particle sizes of (a)-(f) are 19, 18, 83, 33, 13, and 29 μm, respectively.

2.2 The synthesis of Al-substituted tobermorite

Six different combinations of oxide powders derived from waste materials were used as starting materials in this study, and the resultant products were

labeled as following: eggshells (ES), rice husks (RH), glass cullet (GC), eggshells - rice husks (ES+RH) and eggshells - glass cullet (ES+GC). The synthesis with reagent-grade oxide powder (MO) was also conducted for comparison purposes. The synthesis condition used in this study was based on the results of previous works [10, 11]. The molar ratios of starting materials were as following: CaO/(SiO₂+Al₂O₃) = 0.83 and Al₂O₃/(Al₂O₃+SiO₂) = 0.15. The chemical compositions were summarized in Table 2.

The amount of NaOH (Technical grade, pellets, 98%, Spolchemie) additive and deionized water (W) was calculated such that the mass Na₂O:(CaO+SiO₂+Al₂O₃) and W: (CaO+SiO₂+Al₂O₃+Na₂O) ratios were equal to 0.1 and 10, respectively. Reagent-grade oxide powders (Ajax Finechem) may be added in the suspension to stoichiometrically adjust the oxide molar ratio of starting materials. Aqueous NaOH solution was first prepared by dissolving NaOH pellets into deionized water, followed by adding other dry mixtures. The suspensions were stirred for 10-20 minutes. The synthesis was carried out in Teflon-lined autoclave (45-ml acid digestion bombs, Parr Instrument Company) at 150°C under atmospheric condition for 48 hrs. Reaction products were then washed repeatedly with deionized water until neutrality and dried at 40°C in air.

2.3 Characterization

The crystalline phases of the products were analyzed by powder X-ray diffraction analysis (XRD) using a Rigaku Miniflex II X-ray diffractometer and CuK α source, and thermogravimetric analysis was performed using a Perkin Elmer TGA7 Differential Thermal Analyzer. Differential scanning calorimetry (DSC) was carried out on a DSC1, Mettler Toledo, STAR^c System. Fourier transform (FT-IR) measurements using Bruker Optics, Vertex70 and Fourier Transform Raman Spectrometer (FT-Raman, Perkin Elmer Spectrum GX) invariably incorporated with Nd:YAG solid state lasers operating at 1064 nm were used to characterize functional groups and structural information. The morphology of reaction

products was examined by scanning electron microscopy (SEM, Camscan MX2000, England). Nitrogen adsorption and desorption isotherms (77 K, Autosorb-iQ Quantachrome instruments and software, USA) were used to evaluate specific surface areas and pore size distributions (BET and BJH methods).

The uptake of Pb²⁺ and Cd²⁺ was determined at room temperature. Pb²⁺ and Cd²⁺ were selected for this study since they are a common constituent of environmental pollutants. 0.025 g of products was allowed to equilibrate in 100 ml Pb(NO₃)₂ or Cd(NO₃)₂ aqueous solution at a concentration of 0.5 mM for 60 hrs under vigorous stirring. The percentage of removal capacity was then determined on the basis of concentration variation of the cations in solution using Inductively Coupled Plasma (ICP, 700 series ICP-OES, Agilent Technologies).

Table 2. Composition of products.

Products	CaO from eggshell (g)	SiO ₂ from rice husk (g)	Glass cullet (g)	SiO ₂ (g)	CaO (g)	Al ₂ O ₃ (g)	NaOH (g)	Deionized water (ml)
MO	-	-	-	0.85	0.78	0.26	0.12	20.00
ES	0.79	-	-	0.85	-	0.26	0.12	20.00
RH	-	0.86	-	-	0.77	0.26	0.12	20.00
GC	-	-	1.32	-	0.59	0.24	0.02	20.00
ES+RH	0.79	0.86	-	-	-	0.26	0.12	20.00
ES+GC	0.60	-	1.32	-	-	0.24	0.02	20.00

MO means products synthesized from reagent-grade oxide powders

3. Results and discussion

The FTIR spectra of different products are shown in Fig. 2. The vibrational spectra of all products consist of three groups of bands: CO₃²⁻ vibration, stretching and bending vibrations of water molecules and O-H groups, and silicate tetrahedral vibrations. The appearance of CO₃²⁻ bands in the spectra of all products might be due to contamination with CO₂ in air or the carbonation of products. Asymmetric stretching of CO₃²⁻ appears as broad bands at 1400–1500 cm⁻¹. The weak band appearing as a low energy tail around ~900 cm⁻¹ is due to the out-of-plane bending of CO₃²⁻. The band at 1632 cm⁻¹ is attributed to the scissoring bending mode of water vibration. The antisymmetric stretching vibration of water and the stretching band of hydroxyls appear as a broad band centered at 3445 cm⁻¹.

The vibrational spectra of silicate tetrahedral are at 400–1200 cm⁻¹ region. A characteristic band near 1200 cm⁻¹ is due to Si–O stretching vibrations in Q³ sites. The complex group of bands in the range of 1100–900 cm⁻¹ is attributed to asymmetrical stretching vibrations of SiO₄⁴⁻ tetrahedra. The assigned band at 963 cm⁻¹ is the main Si–O band of the tobermorite (Si–O stretching of Q² sites). The intensity of this band is greater for ES than in other products, indicating the existence of a large amount of tobermorite phase. The broad bands in the 556–400 cm⁻¹ region are characterized as O–Si–O deformation or

bending modes. The band at ~672 cm⁻¹ is due to Si–O–Si bending vibrations.

The differential thermal analysis (DTA) is examined from 50 to 450°C, and the patterns are shown in Fig. 3. Tobermorite, generally, exhibits endothermic peak due to dehydration at about 200°C [12]. This peak can be, however, shifted towards lower temperature with higher degree of structural disorder or with the presence of other low temperature-stable phases such as calcium silicate hydrate or calcium aluminate hydrate. The results show that the peaks corresponding to the tobermorite dehydration are shifted to lower temperatures depending upon the amount of tobermorite phase. An intermediate-temperature endotherm at about 400°C reflects a loss of water in katoite structure [13], which is significantly found in RH, GC, and ES+RH products. Katoite normally starts dehydrating at 300–350°C forming C₃AH_{1.5} before undergoing complete dehydration around 500°C.

The crystalline structures of above compounds are identified in the XRD spectra, as shown in Fig. 4. The interplanar distance, *d*, of the characteristic diffraction peak at 2-theta ~ 7.8° in MO and ES products is approximately equal to 11 Å, confirming the formation of 11 Å tobermorite [14]. Hydrothermal processing of RH, GC, ES+RH and ES+GC, however, gives rise to a shift in such peak toward lower 2-theta along with a smaller quantity of tobermorite formation. In addition, XRD analysis reveals that these products composed of the hydrogarnet, katoite, as indicated in the XRD and DTA

patterns. The parent phase, quartz, was also detected in ES+RH in significant quantity. The peak at 29.4° is found to be calcium carbonate, which is derived from the atmospheric carbonation of CaO. The remaining C-S-H may also contribute in this peak. Previous researches [11, 15] have found that the formation of C-S-H takes place in the intermediate stage according to the scheme: $\text{CaO} + \text{SiO}_2 + \text{H}_2\text{O} (+ \text{NaOH}) \rightarrow \text{C-S-H} \rightarrow \text{C-S-H} + \text{tobermorite gel} \rightarrow \text{C-S-H} + \text{tobermorite}$. For RH sample, however, the Raman spectra demonstrate that the main component is calcium carbonate.

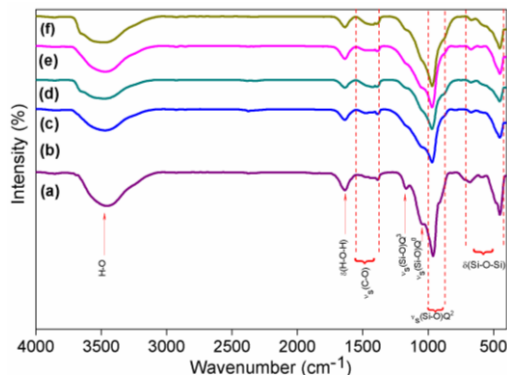


Fig. 2. FTIR spectra of (a) MO, (b) ES, (c) RH, (d) GC, (e) ES+RH and (f) ES+GC.

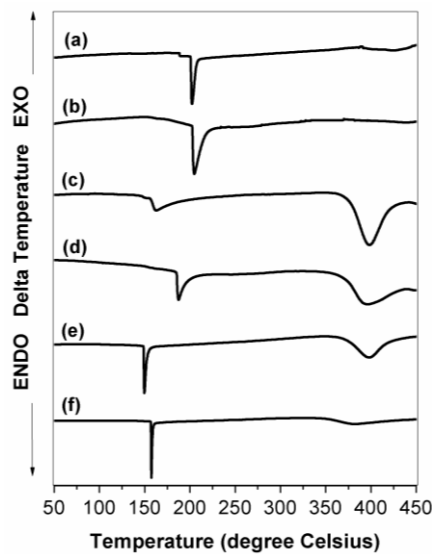


Fig. 3. DSC data for products synthesized from (a) MO, (b) ES, (c) RH, (d) GC, (e) ES+RH and (f) ES+GC.

Fig. 5 illustrates Raman spectra of the products. From the results, it can be seen that ES shows better resolved and well-defined Si-O bands than other products, indicating an ordered crystal structure. The peaks centered at 972 and 1016 cm^{-1} can be assigned to Si-O asymmetric and symmetric stretching vibration of Q^2 tetrahedra. The peak near 683 cm^{-1} is assigned to Si-O-Si bending involving Q^2 tetrahedra. The broad band at 1080 cm^{-1} is attributed to the overlapping of the vibration of carbonate group derived from atmospheric carbonation process and

Si-O symmetrical stretching of Q^3 tetrahedra. The spectra of vibrations involving Ca-O polyhedra at 278 cm^{-1} and C-O-C bending at 710 cm^{-1} in carbonate groups confirm the existence of calcite in this sample. In consistent with FTIR results, it is obvious that ES has a predominant Q^2 peaks rather than other products. Although typical tobermorite contains bridging Q^3 and paired Q^2 sites, FTIR and Raman studies detect significant amount of Q^1 sites, indicating the presence of tetrahedral defects in disordered products [16]. Reaction products synthesized from a mixture of wastes, on the other hands, consist of a number of broad peaks, which reflect the variation in the Si sites and the degree of disorder within the structure.

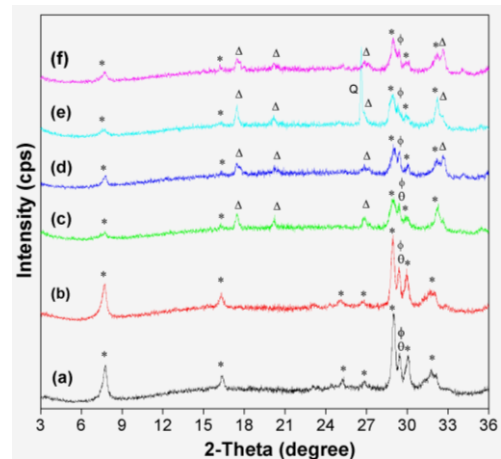


Fig. 4. Powder XRD patterns of (a) MO, (b) ES, (c) RH, (d) GC, (e) ES+RH and (f) ES+GC; * = tobermorite ($\text{Ca}_5\text{Si}_6\text{O}_{18}\text{H}_2 \cdot 4\text{H}_2\text{O}$), Δ = katoite ($\text{Ca}_3\text{Al}_2\text{SiO}_{12}\text{H}_8$), θ = calcite (CaCO_3), ϕ = calcium silicate hydrate (C-S-H), and Q = quartz (SiO_2).

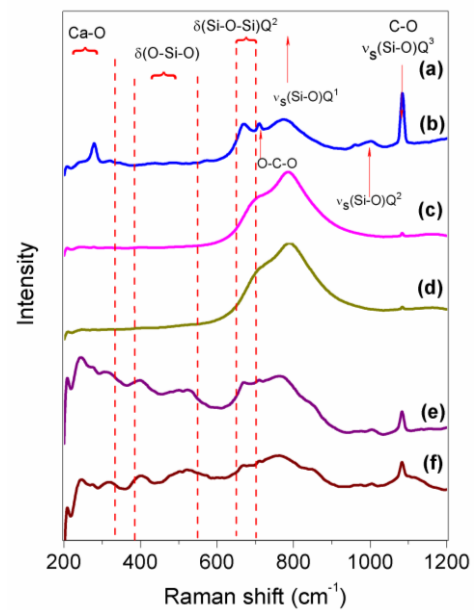


Fig. 5. Raman spectra of (a) MO, (b) ES, (c) RH, (d) GC, (e) ES+RH and (f) ES+GC. In the case of MO, ES, GC, and ES+RH, the intensity was multiplied by 3, 17, 6, 14 and 17, respectively.

SEM micrographs of tobermorite products prepared by hydrothermal treatment for 48 h are shown in Fig. 6. The prominent difference between morphologies of different tobermorite products could be observed. Large lath-like crystallites with a length of several micrometers are evidently observed in MO and ES products, while RH,

GC, ES+RH, and ES+GC exhibit smaller lath-like or platy crystallites. The difference in morphology is reportedly a function of the extent of Al substitution [17]. Lower degree of Al substitution in the tobermorite structure of this sample is due to the involvement of Al in the katoite ($\text{Ca}_3\text{Al}_2\text{SiO}_{12}\text{H}_8$) structure of these products.

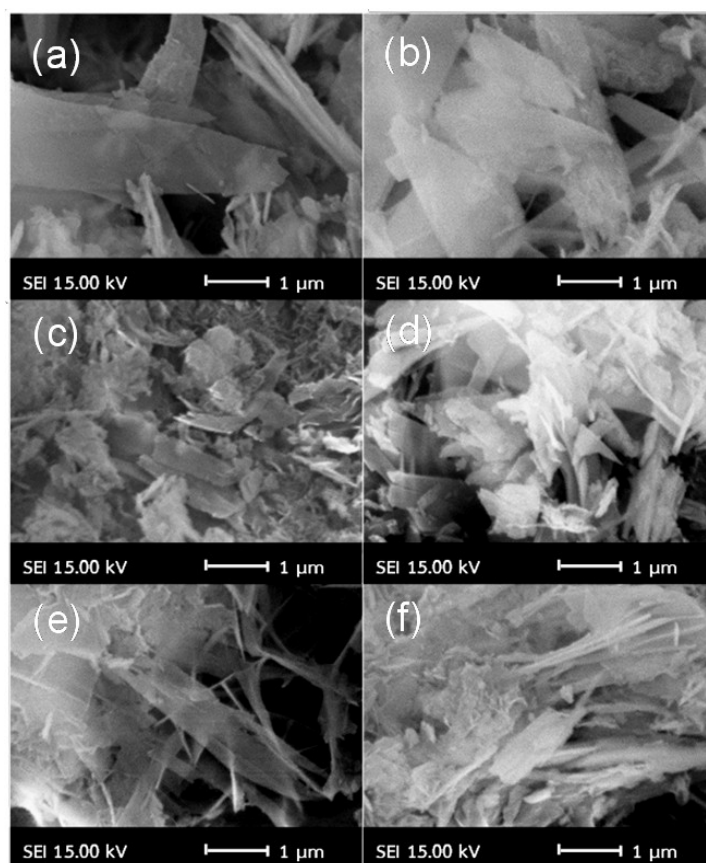


Fig. 6. SEM micrographs of (a) MO, (b) ES, (c) RH, (d) GC, (e) ES + RH and (f) ES + GC.

The specific surface area was determined from N_2 adsorption-desorption isotherm using BET method (Table 3). The sorption isotherms (Fig. 7) of all products can be classified as Type I, which is a characteristic of materials with microporous structure. Large adsorption at high relative pressure ($P/P_0 > 0.9$) indicates the presence of macropores. The BET surface areas of MO, ES, RH, and

ES + RH products were in the range of $70\text{--}80\text{ m}^2\text{ g}^{-1}$, confirming that these wastes can be used as effective raw materials with a small effect on specific surface areas. The effect of glass cullet raw material, however, is to significantly decrease the specific surface area less than $45\text{ m}^2\text{ g}^{-1}$. This could be due to the presence of trace amounts of impurities in this waste.

Table 3. BET specific surface area, pore volume, average pore size, and metal ion uptake of products.

Products	Pore volume (cc g^{-1})	Average pore size (Å)	BET specific surface area ($\text{m}^2\text{ g}^{-1}$)	Cd^{2+} uptake at 60 hrs. (mg g^{-1})	Pb^{2+} uptake at 60 hrs. (mg g^{-1})
MO	1.80	979.0	73.5	133	413
ES	0.84	430.0	77.0	122	414
RH	0.63	316.0	79.5	132	398
GC	0.25	269.8	37.6	82.0	299
ES + RH	0.74	370.5	79.9	151	389
ES + GC	0.29	269.8	43.6	100	304

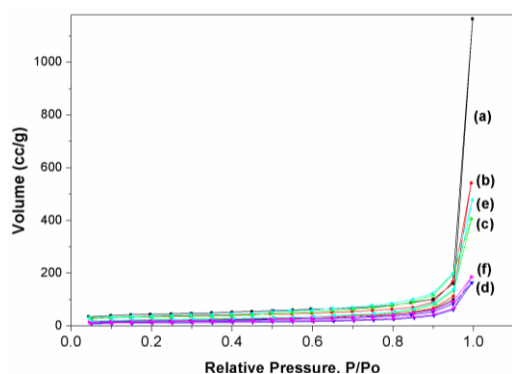


Fig. 7. N_2 sorption isotherms of (a) MO, (b) ES, (c) RH, (d) GC, (e) ES + RH and (f) ES + GC.

Based on above results, the presence of impurities in wastes such as glass cullet could inhibit the crystallization and lower the specific surface area of desirable tobermorite products. A large amount of 11 Å tobermorite could be obtained from the use of eggshell-derived CaO as a starting raw material. It is expected that a lower amount of tobermorite in RH could be due to the larger particle size of SiO_2 powders prepared from rice husk wastes (Fig. 1). Kikuma et al. [18] have reported that the dissolution of SiO_2 in solution phase during the reaction period decreases with increasing SiO_2 particle size. This results in high Ca ion concentration and inhibits the formation of tobermorite.

The removal capacities of Pb^{2+} and Cd^{2+} is listed in Table 3. The results demonstrate that the uptakes of Pb^{2+} and Cd^{2+} are of the following order: MO, ES > RH > ES+RH > ES+GC > GC and ES+RH > MO, RH > ES > ES+GC > GC, respectively. It is found that MO and ES with a large amount of a crystalline-tobermorite ion exchanger have the highest Pb^{2+} removal capacity. ES+RH with less crystalline tobermorite, on the other hand, has relatively higher uptake of Cd^{2+} than MO and ES products. This discrepancy is consistent with previous work, which has reported that low crystallinity of tobermorite could assist the transport and ion-exchange of Cd^{2+} [19]. The inferior performance of GC and ES+GC in ion-uptake behavior could be explained by their much lower specific surface area and amount of tobermorite. Nevertheless, the removal capacities of biomass waste-derived tobermorite (RH, ES, and ES+RH) towards Pb^{2+} and Cd^{2+} is more effective than the use of biomass adsorbents [19, 20].

4. Conclusions

11 Å Al-substituted tobermorite was successfully and hydrothermally synthesized from waste materials under optimal condition; 150°C for 48 hours, molar ratio of CaO / ($SiO_2 + Al_2O_3$) = 0.83 and $Al_2O_3 / (Al_2O_3 + SiO_2)$ = 0.15. A large amount of 11 Å tobermorite could be synthesized by using eggshell-derived CaO starting material. The results showed that the ion-uptake capacities of the products prepared from wastes compared well with those of reagent oxide-derived tobermorite.

Acknowledgements

The authors wish to thank Department of Materials Science and Engineering, Faculty of Engineering and Industrial Technology, Silpakorn University, and National Center of Excellence for Petroleum, Petrochemicals and Advanced Materials for supporting and encouraging this investigation.

References

- [1] J. J. Thomas, H. M. Jennings, A. J. Allen, *Journal of Physical Chemistry C* **114**, 7594 (2010).
- [2] S. Brunauer, *American Scientist* **50**, 210 (1962).
- [3] S. Diamond, J. L. White, W. L. Dolch, *American Mineralogist* **51**, 388 (1966).
- [4] S. Komarneni, D. M. Roy, *Science* **221**, 647 (1983).
- [5] T. Mitsuda, *Mineralogical Journal* **6**, 143 (1970).
- [6] R. Siauciunas, V. Janickis, D. Palubinskaite, R. Ivanauskas, *Ceramics-Silikaty* **48**, 76 (2004).
- [7] N. J. Coleman, *Materials Research Bulletin* **40**, 2000 (2005).
- [8] N. J. Coleman, *Separation and Purification Technology* **48**, 62 (2006).
- [9] N. Y. Mostafa, A. A. Shaltout, H. Omar, S. A. Abo-El-Enein, *Journal of Alloys and Compounds* **467**, 332 (2009).
- [10] S. Shaw, S. M. Clark, C. M. B. Henderson, *Chemical Geology* **167**, 129 (2000).
- [11] T. Ngoyjansri, P. Yantreesingha, S. Leelawannakhet, *Feasibility Study on Hydrothermal Synthesis of Ca-Si-O Materials for Wastewater Treatment*. Senior Project Thesis, Department of Materials Science and Engineering, Silpakorn University, Thailand (2013).
- [12] S. N. Ghosh, *Advances in Cement Technology: Chemistry Manufacture and Testing*, Taylor & Francis (2003).
- [13] C. A. Ríos, C. D. Williams, M. A. Fullen, *Applied Clay Science* **43**, 228 (2009).
- [14] N. J. Coleman, C. J. Trice, J. W. Nicholson, *International Journal of Mineral Processing* **93**, 73 (2009).
- [15] G. Matekonis, R. Šiaučiūnas, D. Vaičiukynienė, *Materials Science* **16**, 242 (2010).
- [16] R. J. Kirkpatrick, J. L. Yarger, P. F. McMillan, P. Yu, X. Cong, *Advanced Cement Based Materials* **5**, 93 (1997).
- [17] S. L. Hoyle, M. W. Grutzeck, *Journal of the American Ceramic Society* **72**, 1938 (1989).
- [18] J. Kikuma, M. Tsunashia, T. Ishikawa, S. Y. Matsuno, A. Ogawa, K. Matsui, *Proceedings of 5th International Conference on Autoclaved Aerated Concrete "Securing a sustainable future"*, Bydgoszcz, 2011.
- [19] N. J. Coleman, Q. Li, A. Raza, *Physicochemical Problems of Mineral Processing* **50**, 5 (2014).
- [20] D. Wankasi, M. Horsfall Jnr, A. Ibuteme Spiff, *Electronic Journal of Biotechnology* **9**, 587 (2006).

*Corresponding author: vorrada@gmail.com